

Effect of Ni Doping on Structural, Optical, and Magnetic Properties of Fe-Doped ZnO Nanoparticles

Raminder Preet Pal Singh¹ · I. S. Hudiara² · Sudhakar Panday¹ · Shashi Bhushan Rana³

Received: 27 May 2015 / Accepted: 23 July 2015 / Published online: 9 September 2015
© Springer Science+Business Media New York 2015

Abstract In the present work, pure ZnO, Zn_{0.99}Fe_{0.01}O (ZFO), Zn_{0.99}Ni_{0.01}O (ZNO) and Zn_{0.98}Fe_{0.01}Ni_{0.01}O (ZFNO) dilute magnetic semiconductors were successfully synthesized by using the wet coprecipitation method. Pure and doped samples were characterized by X-ray diffraction, scanning electron microscopy, energy-dispersive X-ray spectroscopy, UV-Vis spectroscopy and vibrating sample magnetometer. The X-ray diffraction (XRD) analysis of pure and doped samples confirms the formation of a hexagonal wurtzite structure, without formation of any other secondary and impurity phases. Surface morphology of pure and doped ZnO nanoparticle samples performed by scanning electron microscopy (SEM) reveals the formation of spherical nanocrystallites with clear and welldefined boundaries. Energy-dispersive X-ray spectroscopy (EDS) indicates the successful substitution of dopant Fe²⁺ and Ni²⁺ in the lattice site of Zn²⁺ and results in the formation of single-phase Zn_{1-x-y}Fe_xNi_yO. The UV-visible absorption spectra of all doped samples showed blueshift in absorption edge as compared to undoped ZnO nanoparticles. The magnetic characterization reveals and confirms the roomtemperature ferromagnetism in all doped and codoped samples. Magnetization saturation is enhanced in Ni–Fe codoped sample as compare with individual Fe and Nidoped

ZnO samples which further reveals that exchange interaction between Fe and Ni ions dominates over the Fe–Fe and Ni–Ni ion interaction.

Keywords Doped and undoped ZnO nanoparticles · XRD · SEM · EDS · UV-visible · Magnetic characterization

1 Introduction

Diluted magnetic semiconductors (DMS) have attracted much attention in recent years because it is a type of semiconductor in which fraction of host cations can be easily replaced by magnetic ions for its potential applications in fabricating spintronic devices such as spin-valve transistor [1–4]. ZnO is a group II–IV compound semiconductor and has become one of the most promising candidates for DMS materials [5]. Moreover, ZnO have potential applications in optoelectronics due to its wide band gap (3.37 eV) and high exciton binding energy (60 meV) properties. In the past few years, scientists are investigating the effect of doping ZnO nanoparticles with transition metals such as Fe, Co, Ni, and Mn. [6–18]. A lot of theories have proposed, predicted, and revealed that doping ZnO nanoparticles with these transition elements results in dramatic change in various luminescent and magnetic properties. These transition metals have been doped on ZnO lattice to change the different optical and magnetic properties, which further have potential applications in spintronic devices, such as spin field effect transistor, gas sensor, and quantum computers. In order to realize these objectives; it is absolutely necessary to create ZnO-based ferromagnetic material, where their physical and structural properties must be well understood explicitly. Experimental studies confirmed that

✉ Shashi Bhushan Rana
shashi_rana12@yahoo.co.in

¹ Department of Electronics & Communication Engineering, Desh Bhagat University, Mandi Gobindgarh, India

² Chitkara University (Punjab Campus), Chandigarh, India

³ Department of Electronics & Communication Engineering, GNDU Regional Campus, Gurdaspur, India

the ferromagnetism strongly depends on synthesis techniques and environmental conditions used for the preparation of samples. A lot of work had been done on single transition metal-doped ZnO prepared by various techniques [19, 20]. There are few reports on codoping of two magnetic elements simultaneously in a host material such as Fe–Co codoped [21], Mn–Co codoped [22], Cr–Fe codoped, and Co–Cu codoped [23]. Wu et al. [24] also synthesized Fe–Ni-codoped ZnO ($\text{Zn}_{0.95}\text{Fe}_{0.03}\text{Ni}_{0.02}\text{O}$) nanorods by a hydrothermal method and reported that room-temperature ferromagnetism for codoped sample is greater than that for single-doped Fe and Ni samples. Various chemical methods have been developed to prepare nanoparticles (NPs) of different materials of interest. Most of the ZnO nanocrystals have been synthesized by traditional high-temperature solid-state reaction method. However, this method is time-consuming and the properties of the product cannot be controlled. Hence, ZnO nanoparticles can be prepared on a large scale at low cost by simple solution-based methods, such as chemical coprecipitation, hydrothermal reaction, and sol-gel synthesis.

In this work, coprecipitation method was chosen for synthesis because it requires less temperature, is cost-effective, and offers larger degree of solubility of dopants. The effect of Fe and Ni and their codoping on the structural, morphological, optical, and magnetic properties on ZnO nanoparticles were investigated by using X-ray diffraction (XRD), scanning electron microscopy (SEM), UV-Vis spectroscopy, and vibrating sample magnetometer (VSM), respectively. It was observed that incorporating Fe and Ni and their codoping on ZnO nanoparticles not only result in increase in ferromagnetic properties in host material but also change the optical properties and lattice constant values in structural studies.

The organization of this research paper is summarized as follows: Section 2 illustrates the experimental procedure followed to synthesize the doped and undoped ZnO nanoparticles, followed by Section 3, which describes the instrumentation used to characterize the structural, morphological, optical, and magnetic properties of undoped and doped ZnO sample. In Section 4, various results have been discussed in detail related to above-said properties, while Section 5 concludes the paper.

2 Experimental Procedure

All the materials used in this work were of analytical reagent grade and we have used them without any further purification. In order to synthesize the pure ZnO nanoparticles, zinc acetate ($\text{Zn}(\text{CH}_3\text{COO})_2 \cdot 2\text{H}_2\text{O}$) was dissolved in distilled water and stirred for 1 h. Aqueous solution of NaOH was added dropwise to the solution to maintain the pH

~ 10 . The solution was then stirred at room temperature for 4 h followed by aging for 24 h at the same temperature. After aging, the precipitate that formed was filtered and washed several times and was finally annealed at 600 °C for 2 h. In order to synthesize the doped ($\text{Zn}_{0.99}\text{Fe}_{0.01}\text{O}$ (ZFO) and $\text{Zn}_{0.99}\text{Ni}_{0.01}\text{O}$ (ZNO)) and codoped sample ($\text{Zn}_{0.98}\text{Fe}_{0.01}\text{Ni}_{0.01}\text{O}$ (ZFNO)) nanocrystals, the same steps have been followed except adding ferric nitrate (FeNO_3) and nickel acetate ($\text{C}_4\text{H}_6\text{NiO}_4 \cdot 4\text{H}_2\text{O}$) according to the calculated stoichiometric ratio.

3 Characterization of Pure and Doped Samples

X-ray diffraction patterns of all the powder samples were recorded by rotating angle X-ray diffractometer (Bruker AXS D8 Advance, Germany) equipped with graphite monochromator, a mirror at a fixed incidence angle of 1°–5° and $\text{CuK}\alpha$ (wavelength = 1.540 Å, 40 kV, 100 mA) radiation source. The angular accuracy of the setup was 0.001° and the angular resolution was about 0.01°. The samples were scanned in an angular direction in the range from 20° to 90° (2θ) with a step size of 0.01°. The surface morphology of undoped (pure) and doped synthesized samples was ascertained by using the scanning electron microscope Carl Zeiss Supra 55 which operates at a high accelerated voltage of 15 kV. The UV absorption spectra of the samples were recorded on the Systronics-2205 double-beam spectrophotometer having a bandwidth 1 nm and wavelength ranges from 200 to 1100 nm. Elemental composition of various sample were ascertained by using energy-dispersive X-ray spectroscopy (EDS) at an acceleration voltage of 200 keV. Magnetic hysteresis loop at room temperature was measured by using a VSM (Microsense EZ9) having a maximum magnetic field strength of 22.5 kOe.

4 Results and Discussions

4.1 XRD Analysis

Figure 1a and b shows the X-ray diffraction patterns of the synthesized undoped (pure ZnO) and doped (ZFO, ZNO and ZFNO) samples. Each XRD sample exhibit the hexagonal wurtzite phase without any impurities and secondary phase formation. It is clear from the XRD pattern that all the characteristic diffraction peaks can be indexed to the diffractions of (100), (002), (101), (102), and (110) planes with a hexagonal wurtzite structure. These diffraction peaks agree well within the values of the standard value of JCPDS01-079-2205 card value. From the XRD pattern of Fig. 1a and b, it is clear that the doped samples show lowering of intensity and the peak position of doped samples shifts to higher angles

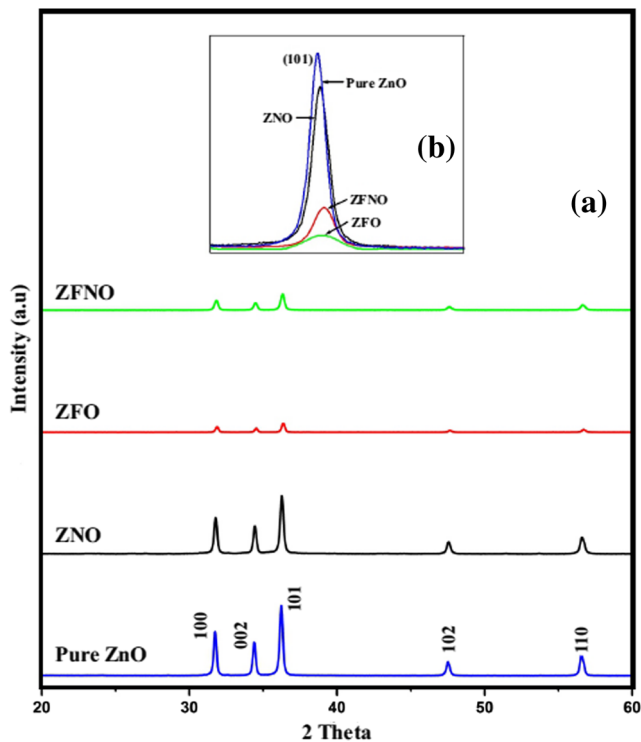


Fig. 1 (a) XRD patterns of pure ZnO, ZFO, ZNO, and ZFNO nanoparticles annealed at 600°, and (b) shifting of (101) peak with the doping concentration

in (101) characteristic peak as compared to undoped (pure) ZnO. It is observed further that the intensity of diffraction peaks decreases markedly as a function of Fe and Ni concentration, signifying that the crystalline character of the ZnO had reduced considerably due to Fe and Ni doping. The XRD spectra clearly show that some XRD peaks appearing in undoped ZnO at higher angles disappear in the Fe-, Ni-, and Fe–Ni-doped ZnO samples. This phenomenon is due to the reduction of grain size and the presence of strain in the ZnO lattice due to induction of Fe, Ni, and Fe–Ni atoms. For codoped sample, NP size reduction is significant as compared to undoped and doped NPs as shown in Table 1.

Figure 1b clearly shows the shifting of peak toward higher 2θ angle value with doping of Fe and Ni and codoping. The change in the peak positions clearly indicates that

Fe and Ni ions are occupying the Zn position in the ZnO matrix [25].

The average crystalline size was calculated by using Scherrer’s (1) and was found to be in the range of 36 to 45 nm as shown in Table 1.

$$\tau = \frac{k\lambda}{\beta \cos \theta} \tag{1}$$

Where, τ is the grain size, β is the full width at half maxima, λ is the wavelength of X-ray used (1.548 Å), and θ is the diffraction angle. Lattice strain and dislocation density increase with doping and codoping as compared with undoped ZnO as shown in Table 1. From the d values, lattice constants a and c are calculated using (2), and their values are given in Table 1.

$$\frac{1}{d^2} = \frac{4}{3} \left(\frac{h^2 + hk + k^2}{a^2} \right) + \frac{l^2}{c^2} \tag{2}$$

The ionic radius values for various elements like Fe³⁺, Ni²⁺, and Zn²⁺ are 67, 69, and 74 pm, respectively. It is clearly observed from Table 1 that value of lattice parameters and d value go on reducing due to the smaller ionic radius of Fe, Ni, and Fe–Ni ions due the substitution of Zn²⁺ by Fe³⁺, Ni²⁺, and Fe–Ni ion during the doping process.

The XRD spectra also show that the intensity of characteristic XRD peaks decreases on changing the doping concentration of these dopants, which further indicates the reduction in crystalline character and decrease in crystallite size as evident from Table 1.

4.2 Scanning Electron Microscope Analysis

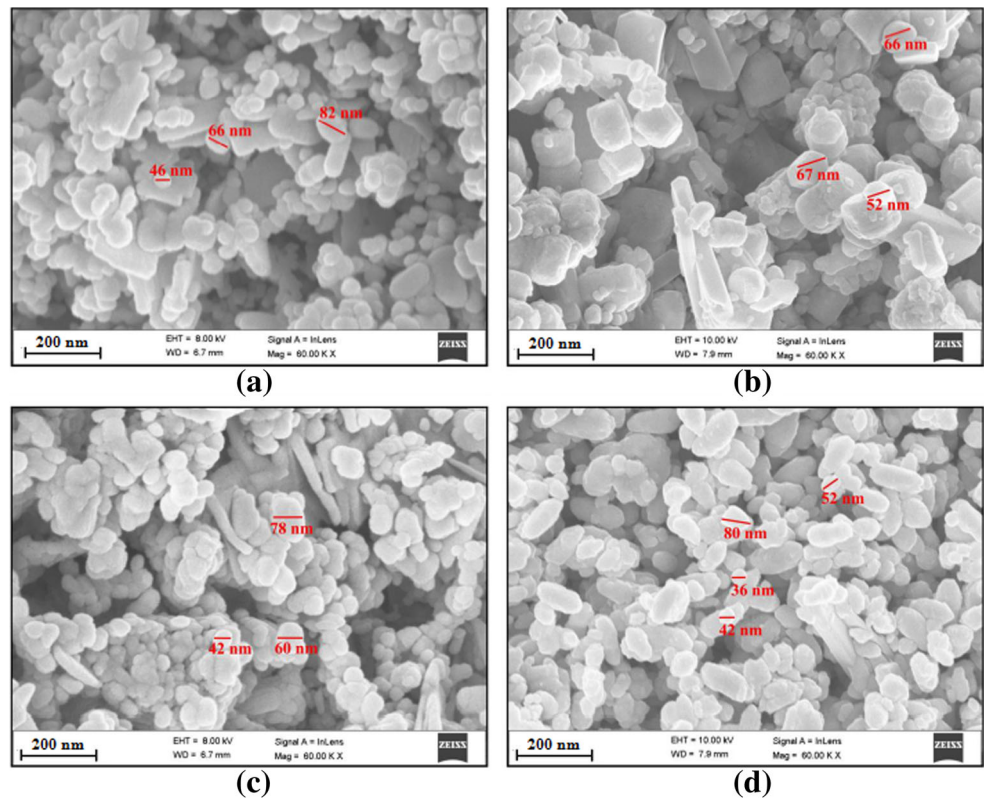
The morphology of pure and doped samples was studied by using the scanning electron microscope (SEM) analysis. Figure 2a–d shows the SEM images of pure ZnO, ZFO, ZNO, and ZFNO nanoparticles with an average particle size of approximately 65, 62, 60, and 53 nm, respectively.

The SEM image of pure ZnO shows that the particles are spherical in shape with large agglomeration. It is clearly found from Fig. 2b–d that the aggregation is almost restricted in doped ZnO (from ZFO to ZFNO) particles which appears in a consistent and uniform shape with constricted size distribution. The particle size measured from

Table 1 Microstructural properties of pure ZnO and ZFO, ZNO, and ZFNO nanoparticles

Sample	Particle size (nm)	Lattice strain	Dislocation density (× 10 ⁻¹⁴ Line ² /m ²)	d ₁₀₁ (Å)	Lattice constant	
					a	c
Pure ZnO	45	0.0027	4.94	2.4768	3.233	5.280
ZFO	43	0.0030	5.41	2.4689	3.223	5.263
ZNO	42	0.0030	5.67	2.4755	3.232	5.278
ZFNO	36	0.0034	7.72	2.4715	3.227	5.269

Fig. 2 SEM images (a–d) of pure ZnO and ZFO, ZNO, and ZFNO nanoparticles



XRD is quite different from the SEM measurement because in SEM, calculation is done by taking the difference of noticeable grain boundaries, whereas in case of XRD, measurements are taken from the crystalline area that reasonably diffracts the X-ray waves.

From Fig. 2b and c, it is clear that particle size goes on decreasing because dopant Fe and Ni are diffusing homogeneously in the different sites and they are clearly visible with less porosity in the background portion. It is clear from SEM micrograph that pure ZnO nanoparticles appears in bigger form, while codoped ZFNO nanoparticles appear in smaller size which verifies the XRD results.

The elemental composition of the synthesized nanoparticles (doped and undoped) was determined from the EDS

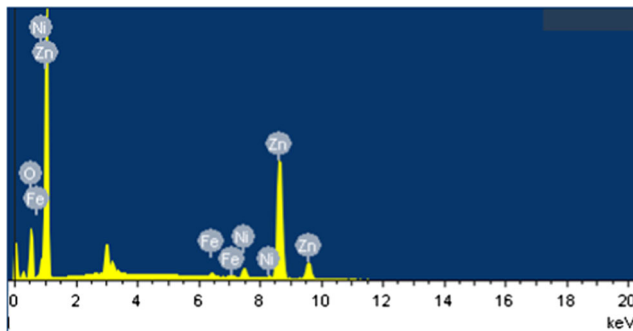


Fig. 3 Energy-dispersive X-ray spectroscopy (EDS) spectrum of ZFNO sample

as shown in Fig. 3. The EDS analysis confirms the presence of Fe, Ni, O, and Zn in the doped sample with no other impurity element.

Figure 3 shows the EDS spectra of ZFNO sample. The EDS spectrum indicates that the synthesized ZFNO sample mainly contains Fe, Zn, Ni, and O elements. The EDS spectral peaks of O appeared at 0.5 keV; Zn appeared at 1, 8.6, and 9.5 keV; while Fe signal appears at 0.6, 6.5, and 7.2 keV,

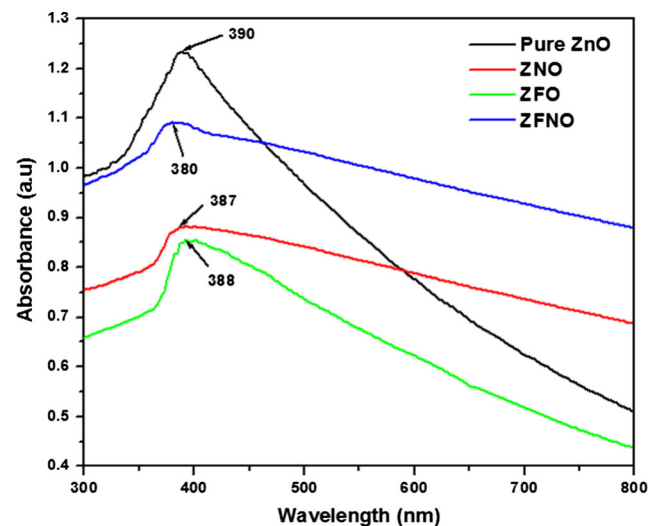


Fig. 4 UV-visible absorption spectra of pure ZnO and ZFO, ZNO, and ZFNO nanoparticles

Table 2 Band gap energy (E_g) variation of pure ZnO and ZFO, ZNO, and ZFNO nanoparticles

Sample	Absorption wavelength (λ), nm	Band gap energy ($E_g = H_c/\lambda$), eV
Pure ZnO	390	3.19
ZFO	388	3.21
ZNO	387	3.22
ZFNO	380	3.27

respectively. The EDS results further verify XRD results, which reveal that Fe- and Ni-doped ZnO magnetic semiconductors were successfully synthesized by the chemical precipitation method.

4.3 Optical Absorption Study

Pure ZnO and doped and codoped ZnO nanoparticles were compared employing UV-visible absorption spectroscopy. The band gap of semiconductor nanoparticles changes as the various dopants can cause different crystal defects on ZnO crystals. The UV-visible absorption study of pure ZnO and doped and codoped ZnO nanoparticle samples has been investigated as shown in Fig. 4 in the wavelength range of

300–800 nm. The value of the absorbance is purely dependent on various factors like the size of particles, flaws, or deformities in grain structure and oxygen deficiency.

As the doping concentration is changed from ZNO, ZFO, and ZFNO, the absorption edge is starting to shift toward lower wavelengths (blueshift) which means the band gap increases which results due to defects (strain) and hence leads to the reduction in crystallite size as discussed in the XRD analysis. Figure 4 shows the absorption spectra of the pure ZnO, ZFO, ZNO, and ZFNO nanoparticles with the absorption peaks at 390, 388, 387, and 380 nm, respectively.

Table 2 summarizes the band gap energy ($E_g = H_c/\lambda$) value for undoped (pure) and doped ZnO nanoparticles. The optical band gap value calculated in our pure ZnO sample is small (3.19 eV) as compared with the standard band gap value of bulk ZnO material, i.e., 3.3 eV. But, the observed E_g value is in good agreement with the E_g value determined in literature [26, 27]. From Table 2, it is concluded that the band gap energy increases with Fe, Ni, and Fe–Ni doping, which shows a blueshift in wavelength.

The increase in band gap from 3.19 to 3.27 eV is due to decrease or reduction in particle size due to changing of various dopants Fe^{+3} , Ni^{+2} , and Fe–Ni, respectively, on ZnO. This phenomenon of increase in band gap energy (E_g) and absorption at the lesser wavelength can be explained on the basis of quantum confinement effect among the individual doped ZnO nanoparticles.

Fig. 5 $M-H$ curve of (a) pure ZnO, (b) ZFO, (c) ZNO, and (d) ZFNO nanoparticles at room temperature

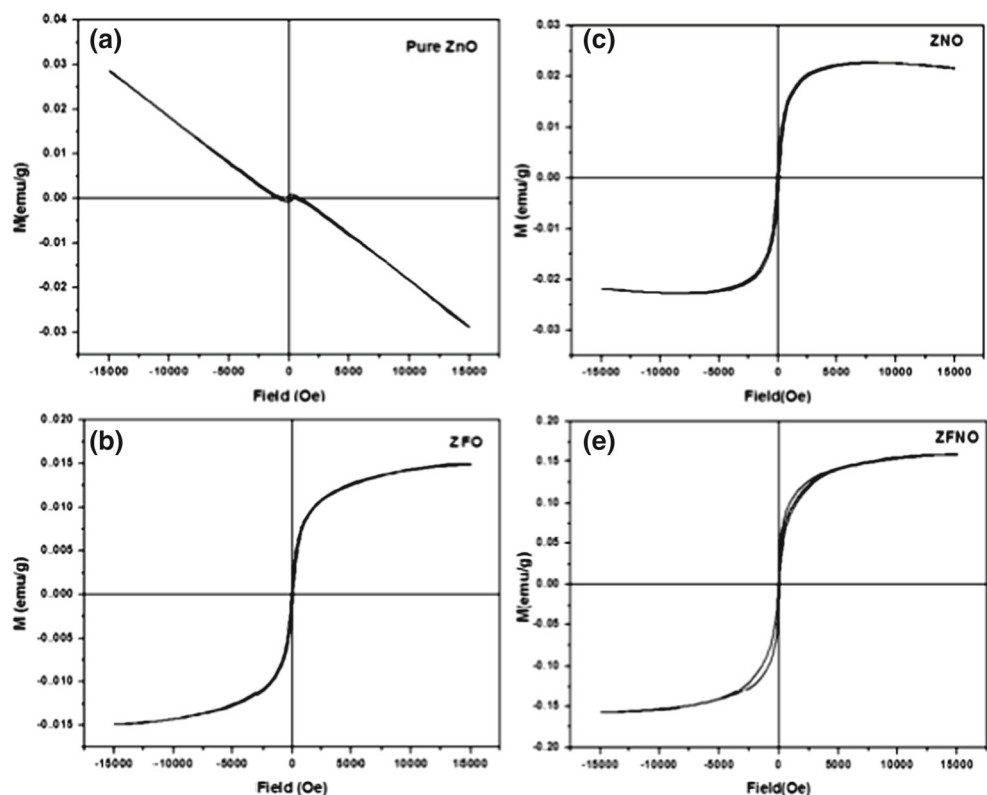


Table 3 Magnetic properties of ZFO, ZNO, and ZFNO nanoparticles

Sample	H_C (Oe)	M_r (emu/g)	M_s (emu/g)
ZFO	61	0.0011	0.015
ZNO	74	0.0027	0.021
ZFNO	51	0.0169	0.158

4.4 Vibrating Sample Magnetometer Analysis

Magnetization measurements of synthesized pure and doped nanoparticles were carried out using a vibrating sample magnetometer by using the magnetic hysteresis ($M-H$) curve. All the measurements were made at room temperature. Pure ZnO sample shows diamagnetic behavior as depicted from Fig. 5a. The diamagnetic nature of pure ZnO has also been reported in literature [28]. Whereas from the magnetic hysteresis loops ($M-H$ curve) for ZFO, ZNO, and ZFNO samples as shown in Fig. 5b–d, respectively, it is clear that all samples exhibit ferromagnetic behavior at room temperature. However, from Table 3, it is clear that magnetization saturation (M_s) and remanent (M_r) is enhanced in ZFNO sample as compare with individual magnetization obtained in ZFO and ZNO samples, whereas coercivity (H_c) is reduced in ZFNO sample in contrast to ZFO and ZNO samples. Moreover, coercivity obtained in all samples is very less which reveals soft ferromagnetic characteristic of samples.

So far, several reasons have been discussed to explain the origin of ferromagnetism and still this subject is controversial. One of the theories proposed that room-temperature ferromagnetism of ZFNO samples is exhibited due to various intrinsic and extrinsic phenomena. Intrinsic phenomenon results due to exchange interaction, and extrinsic phenomenon occurs due to formation of clusters or secondary phases of dopant semiconductor atoms [29]. The relationship between intrinsic defects such as oxygen or Zn vacancies and magnetism is also discussed in some studies [30, 31]. In our study, the XRD and EDS results showed that dopant ions are successfully incorporated in the Zn wurtzite lattice without formation of any secondary phases and metallic clusters. Therefore, the possibility of ferromagnetism due to formation of secondary phases and metallic clusters is completely ruled out in case of our all doped and codoped samples.

Among different mechanisms responsible for ferromagnetism, the oxygen-mediated exchange interaction between the dopant ions could be the possible mechanism responsible for the observed ferromagnetic behavior in all the doped samples. In a recent paper, Das et al. [32] proposed that exchange interaction mechanism mediated by oxygen vacancies is responsible for enhancement in magnetic saturation when Ni is codoped in Mn-doped ZnO

sample because codoping increases carrier concentration in the form of oxygen vacancies.

From XRD, EDS, and VSM analysis of our samples, it is reasonable to say that observed room-temperature ferromagnetism in our samples is an intrinsic property of material and not due to the formation of any secondary phases or metallic clusters. Further, increase in magnetic saturation of codoped sample indicates that Ni–O–Ni and Ni–O–Fe exchange interaction in ZFNO sample dominates the Fe–O–Fe and Ni–O–Ni exchange interaction in case of ZFO and ZNO respectively. Therefore, we conclude that magnetic saturation increases with simultaneous doping of two different transition metals, i.e., Fe–Ni, codoping than single transition metal (Fe, Ni) doping at room temperature. So in our discussion, resulting paramagnetism is an intrinsic property of ZFNO samples.

5 Conclusions

In our investigations, pure ZnO and $Zn_{0.99}Fe_{0.01}O$, $Zn_{0.99}Ni_{0.01}O$, and $Zn_{0.98}Fe_{0.01}Ni_{0.01}O$ diluted magnetic semiconductor nanoparticles were successfully synthesized via a simple coprecipitation method X-ray diffraction pattern shows formation of hexagonal wurtzite structure for all samples. UV absorption spectrum shows blueshift in wavelength for doped and codoped samples as compared with undoped ZnO. The present work also confirms that the optical absorption and band gap of ZnO nanoparticles can be controlled by Fe, Ni, and Fe–Ni doping. Enhancement in roomtemperature ferromagnetism has been observed in Fe–Nidoped ZnO sample as compared with Fe and Nidoped ZnO samples. A few assumptions related to exhibition of roomtemperature ferromagnetism have been addressed i.e. clusters, secondary phase and defectrelated ferromagnetism. However, we believe that a small amount of Fe, Ni and Fe–Ni have played a vital role in order to obtain the roomtemperature ferromagnetism. Oxygenmediated exchange interaction could be the possible mechanism for observed ferromagnetism. In the codoped sample, Ni–O–Ni and Ni–O–Fe carriermediated exchange interaction dominates the Fe–O–Fe and Ni–O–Ni exchange interaction which results in an increase in the value of saturation magnetization at room temperature, which is the best probable mechanism for origination of roomtemperature ferromagnetism.

References

1. Wolf, S.A., Awschalom, D.D., Buhrman, R.A., Daughton, J.M., Von Molnar, S., Roukes, M.L., Chichekanova, A.Y., Treger, D.M.: Spintronics: A spin-based electronics vision for the future. *Science* (2001). doi:10.1126/science.1065389

2. Ohno, H.: Making nonmagnetic semiconductors ferromagnetic. *Science* (1998). doi:[10.1126/science.281.5379.951](https://doi.org/10.1126/science.281.5379.951)
3. Prinz, G.A.: Magnetolectronics. *Science* (1998). doi:[10.1126/science.282.5394.1660](https://doi.org/10.1126/science.282.5394.1660)
4. Ghosh, S., Mandal, K.: Study of $Zn_{1-x}Co_xO$ ($0.02 < x < 0.08$) dilute magnetic semiconductor prepared by mechano-synthesis route. *J. Magn. Magn. Mater.* (2010). doi:[10.1016/j.jmmm.2010.01.017](https://doi.org/10.1016/j.jmmm.2010.01.017)
5. Dietl, T., Ohno, H., Matsukura, F., Cibert, J., Ferrand, D.: Zener model description of ferromagnetism in zinc-blende magnetic semiconductors. *Science* (2000). doi:[10.1103/10.1126/science.287.5455.101](https://doi.org/10.1103/10.1126/science.287.5455.101)
6. Wesselinowa, J.M., Aposto, A.T.: A possibility to obtain room temperature ferromagnetism by transition metal doping of ZnO nanoparticles. *J. Appl. Phys.* (2010). doi:[10.1063/1.3329457](https://doi.org/10.1063/1.3329457)
7. Karmakar, D., Mandal, S.K., Kadam, R.M., Paulose, P.L., Rajarajan, A.K., Nath, T.K., Das, A.K., Dasgupta, I., Das, G.P.: Ferromagnetism in Fe-doped ZnO nanocrystals: Experiment and theory. *Phys. Rev. B* (2007). doi:[10.1103/PhysRevB.75.144404](https://doi.org/10.1103/PhysRevB.75.144404)
8. Xingyan, X., Chuanbao, C.: Structure and ferromagnetic properties of Co-doped ZnO powders. *J. Magn. Magn. Mater.* (2009). doi:[10.1016/j.jmmm.2009.01.017](https://doi.org/10.1016/j.jmmm.2009.01.017)
9. Martínez, B., Sandiumenge, F., Balcells, L., Arbiol, J., Sibiude, F., Monty, C.: Structure and magnetic properties of Co-doped ZnO nanoparticles. *Phys. Rev. B* (2005). doi:[10.1103/PhysRevB.72.165202](https://doi.org/10.1103/PhysRevB.72.165202)
10. Duan, L.B., Rao, G.H., Yu, J., Wang, Y.C.: Ferromagnetism of lightly Co-doped ZnO nanoparticles. *Solid State Commun.* (2008). doi:[10.1016/j.ssc.2008.01.014](https://doi.org/10.1016/j.ssc.2008.01.014)
11. Luo, J., Liang, J.K., Liu, Q.L., Liu, F.S., Zhang, Y., Sun, B.J., Rao, G.H.: Structure and magnetic properties of Mn-doped ZnO nanoparticles. *J. Appl. Phys.* (2005). doi:[10.1063/1.1873058](https://doi.org/10.1063/1.1873058)
12. Wang, J.B., Huang, G.J., Zhong, X.L., Sun, L.Z., Zhou, Y.C., Liu, E.H.: Raman scattering and high temperature ferromagnetism of Mn-doped ZnO nanoparticles. *Appl. Phys. Lett.* (2006). doi:[10.1063/1.2208564](https://doi.org/10.1063/1.2208564)
13. Jayakumar, O.D., Gopalakrishnan, I.K., Sudakar, C., Kadam, R.M., Kulshreshtha, S.K.: Magnetization and structural studies of Mn doped ZnO nanoparticles: Prepared by reverse micelle method. *J. Cryst. Growth* (2007). doi:[10.1016/j.jcrysgro.2006.12.030](https://doi.org/10.1016/j.jcrysgro.2006.12.030)
14. Bhuiyan, M.R.A., Rahman, M.K.: Synthesis and characterization of Ni doped ZnO nanoparticles. *I. J. Eng. Manuf.* (2014). doi:[10.5815/ijem.2014.01.02](https://doi.org/10.5815/ijem.2014.01.02)
15. Vijayaprasath, G., Murugan, R., Ravi, G.: Structural, optical and magnetic properties of Ni doped ZnO nanostructures prepared by co-precipitation method. In: *J. Chem. Tech. Res.* **6**, 3385–3387 (2014)
16. Katoon, S., Ahmad, T.: Synthesis, optical and magnetic properties of Ni-doped ZnO nanoparticles. *J. Mater. Sci. Eng B* **2**(6), 325–333 (2012)
17. Jadhav, J., Patange, M., Biswas, S.: Ferromagnetic Ni-doped ZnO nanoparticles synthesized by a chemical precursor method. *Carbon – Sci. Tech.* **5**(2), 269–274 (2013)
18. John Kennady Vethanathan, S., Perumal, S., Meenakshi Sundar, S., Priscilla Koilpillai, D., Karpagavalli, S., Suganthi, A.: Structural and magnetic properties of nickel and cobalt doped ZnO nanoparticles synthesized by solvothermal route. *Int. J. Adv. Sci. Tech. Res.* **6**(3), 856–865 (2014)
19. Mandal, S.K., Das, A.K., Nath, T.K., Karmakar, D., Satpati, B.: Microstructural and magnetic properties of ZnO: TM (TM = Co, Mn) diluted magnetic semiconducting nanoparticles. *J. Appl. Phys.* (2006). doi:[10.1063/1.2360387](https://doi.org/10.1063/1.2360387)
20. Bilecka, I., Luo, L., Djerdj, I., Rossell, M.D., Jagodi, M., Jaglicic, Z., Masubuchi, Y., Kikkawa, S., Niederberger, M.: Microwave-assisted nonaqueous sol–gel chemistry for highly concentrated ZnO-based magnetic semiconductor nanocrystals. *J. Phys. Chem. C* (2011). doi:[10.1021/jp108050w](https://doi.org/10.1021/jp108050w)
21. Yu, X., Meng, D., Liu, C., He, X., Wang, Y., Xie, J.: Structure and ferromagnetism of Fe-doped and Fe- and Co-codoped ZnO nanoparticles synthesized by homogeneous precipitation method (2012). doi:[10.1016/j.matlet.2012.07.040](https://doi.org/10.1016/j.matlet.2012.07.040)
22. Sharma, V.K., Najim, M., Srivastava, A.K., Varma, G.D.: Structural and magnetic studies on transition metal (Mn, Co) doped ZnO nanoparticles. *J. Magn. Magn. Mater.* (2012). doi:[10.1016/j.jmmm.2011.08.061](https://doi.org/10.1016/j.jmmm.2011.08.061)
23. Chand, P., Gaur, A., Kumar, A.: Effect of Cr and Fe doping on the structural and optical properties of ZnO nanostructures. *Int. J. Chem. Nucl. Mater. Metall. Eng.* **8**, 1238–1241 (2014)
24. Wu, X., Wei, Z., Zhang, L., Zhang, C., Yang, H., Jiang, J.: Synthesis and characterization of Fe and Ni co-doped ZnO nanorods synthesized by a hydrothermal method. *Ceram. Int.* **40**, 14635–14640 (2014)
25. Kumar, S., Kim, Y.J., Koo, B.H., Choi, H., Lee, C.G.: Ferromagnetism in chemically-synthesized Co-doped ZnO. *J. Korean Phys. Soc.* **55**(3), 1060–1064 (2009)
26. Aydın, C., Abd El-Sadek, M.S., Zheng, K., Yahia, I.S., Yakuphanoglu, F.: Synthesis, diffused reflectance and electrical properties of nanocrystalline Fe-doped ZnO via sol–gel calcination technique. *Opt. Laser Technol.* **48**, 447–452 (2013)
27. Morales, A.E., Mora, E.S., Pal, U.: Use of diffuse reflectance spectroscopy for optical characterization of un-supported nanostructures. *Revista Mexicana de Fisica Supplement* **53**, 18–22 (2007)
28. Zhou, S., Potzger, K., Reuther, H., Kuepper, K., Skorupa, W., Helm, M., Fassbender, J.: Absence of ferromagnetism in V-implanted ZnO single crystals. *J. Appl. Phys.* **101**, 09H109 (2007)
29. Sharma, V.K., Varma, G.D.: Fe clusters as origin of ferromagnetism in hydrogenated $Zn_{1-x}Fe_xO$ ($x = 0.02$ & 0.05) samples. *Adv. Mat. Lett.* (2012). doi:[10.5185/amlett.2011.7283](https://doi.org/10.5185/amlett.2011.7283)
30. Bappaditya Pal, G.iri., P.K.: Defect mediated magnetic interaction and high Tc ferromagnetism in Co doped ZnO nanoparticles. *J. Nanosci. Nanotechnol.* **11**, 1–8 (2011)
31. Santara, B., Giri, P.K., Dhara, S., Imakita, K., Fujii, M.: Oxygen vacancy-mediated enhanced ferromagnetism in undoped and Fe-doped TiO_2 nanoribbons. *J. Appl. Phys. Phys. D* (2014). doi:[10.1088/0022-3727/47/23/235304](https://doi.org/10.1088/0022-3727/47/23/235304)
32. Das, J., Mishra, D.K., Sahu, D.R., Roul, B.K.: Influence of Ni doping on magnetic behavior of Mn doped ZnO. *Mater. Lett.* **65**(4), 598–601 (2011)